JCI insight

RESEARCH ARTICLE

Mst1-mediated phosphorylation of Bcl-xL is required for myocardial reperfusion injury

Michinari Nakamura,[1] Peiyong Zhai,[1] Dominic P. Del Re,[1] Yasuhiro Maejima,[1,2] and Junichi Sadoshima[1]

[1]Department of Cell Biology and Molecular Medicine, Cardiovascular Research Institute, Rutgers New Jersey Medical School, Newark, New Jersey, USA. [2]Department of Cardiovascular Medicine, Tokyo Medical and Dental University, Tokyo, Japan.

Mst1 is a central Ser-Thr kinase in the Hippo pathway, which promotes apoptosis and inhibits cell proliferation. We have shown previously that, in cardiomyocytes, oxidative stress activates Mst1 at mitochondria, where Mst1 phosphorylates Bcl-xL at Ser14, inducing dissociation of Bcl-xL from Bax and thereby promoting apoptosis. However, the functional significance of Ser14 phosphorylation of endogenous Bcl-xL in vivo remains elusive. We generated knockin (KI) mice in which Ser14 of Bcl-xL is replaced with Ala. KI mice were born at the expected Mendelian ratio, and adult KI mice exhibited normal cardiac morphology and function at baseline. However, KI mice were protected from myocardial ischemia/reperfusion (I/R) injury and exhibited reduced cardiomyocyte apoptosis. Although suppression of endogenous Mst1 also reduced I/R injury, there was no additive protective effect when Mst1 was inhibited in KI mice. The development of dilated cardiomyopathy induced by cardiac-specific overexpression of Mst1 was also ameliorated in KI mice. Lats2 and YAP, two other key components of the Hippo pathway, were not affected in KI mice. These results suggest that Ser14 phosphorylation of Bcl-xL plays an essential role in mediating both cardiomyocyte apoptosis and myocardial injury by acting as a key downstream mediator of Mst1 independently of the canonical Hippo pathway.

Introduction

Mst1, mammalian Ste20-like kinase 1, is a ubiquitously expressed Ser-Thr kinase. It is one of the most strongly activated kinases in the heart when cardiomyocytes undergo apoptosis, such as under conditions of ischemia/reperfusion–induced (I/R-induced) oxidative stress and in patients with dilated cardiomyopathy (DCM) or arrhythmogenic cardiomyopathy (1–3). We have shown previously that suppression of Mst1 attenuates myocardial injury after I/R as well as the development of heart failure in response to pressure overload and during cardiac remodeling after myocardial infarction (1, 4, 5). Understanding the underlying molecular mechanisms by which Mst1 promotes cardiomyocyte death would allow for the development of innovative treatments for patients with heart disease.

Mst1 is a key component of the Hippo signaling pathway, an evolutionarily conserved and an important signaling pathway that regulates organ size (6–11). Activation of Mst1 and the Hippo pathway, and consequent inhibition of YAP, a nuclear cofactor, stimulates apoptosis, inhibits cell proliferation, and limits organ size in mammals. Increasing lines of evidence suggest that stress-induced activation of Mst1 leads to phosphorylation of several components of the Hippo signaling pathway, including the nuclear Dbf2-related (NDR) family kinases, large tumor suppressor kinase 1/2 (Lats1/2), SAV1, and Lats1/2-interacting adaptor proteins MOBKL1A/1B (MOB1) (12–14). In particular, Lats2 is a direct downstream target of Mst1, both of which make up the canonical Hippo pathway together with YAP, thereby regulating cell proliferation and heart size during cardiac development (9, 15).

Importantly, Mst1 also phosphorylates other substrates that may not belong to the canonical Hippo signaling pathway by forming a unique signaling complex at various subcellular localizations. For example, Mst1 phosphorylates the Ser14 residue in the BH4 domain of Bcl-xL at the outer mitochondrial membrane in cardiomyocytes, which induces the dissociation of Bcl-xL from B cell leukemia/lymphoma 2–associated (Bcl-2–associated) protein x (Bax) and promotes apoptosis by allowing Bax to become active (16). Bcl-xL

Conflict of interest: The authors have declared that no conflict of interest exists.

Submitted: December 23, 2015
Accepted: March 18, 2016
Published: April 21, 2016

Reference information:
JCI Insight. 2016;1(5):e86217.
doi:10.1172/jci.insight.86217.

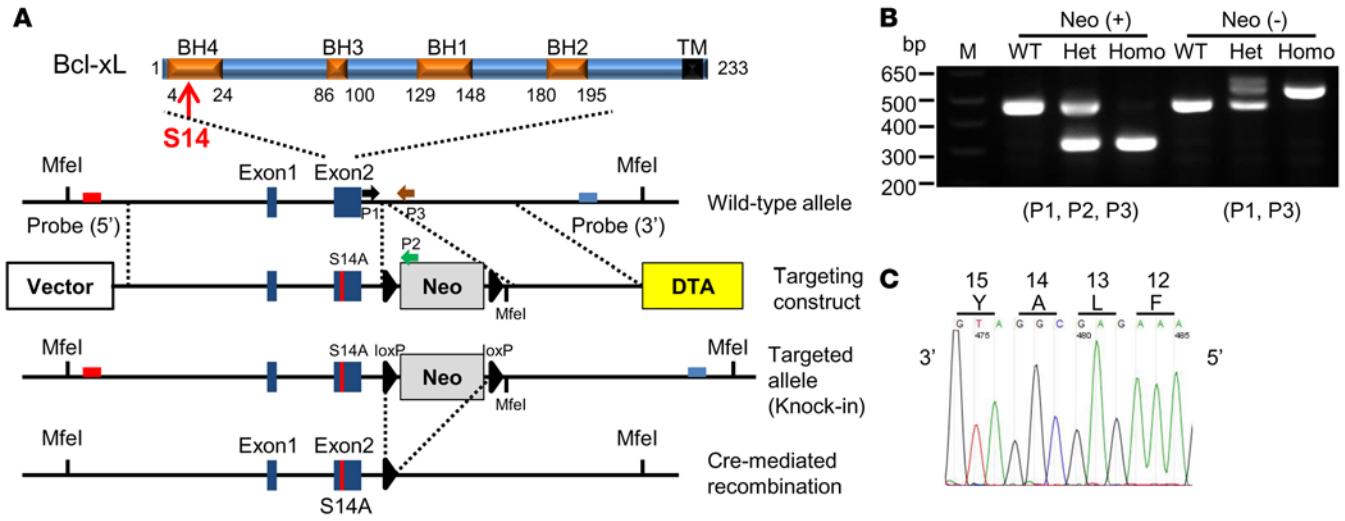

Figure 1. Generation of Bcl-xL S14A knockin mice. (**A**) Schematic diagram of Bcl-xL protein. The arrow shows Ser14. The Bcl-xL genomic region of interest, the targeting construct, and the mutated S14A locus after homologous recombination and Cre-mediated recombination are shown. A neomycin cassette and diphtheria toxin A were used for positive and negative selections, respectively. (**B**) PCR using tail DNA isolated from WT, heterozygous, and homozygous mice, including a neomycin cassette after Cre-mediated recombination. Locations of the primers, P1, P2, and P3 are shown in **A**. M, 100-bp DNA ladder. (**C**) Incorporation of S14A mutation into KI mice was verified by PCR and sequencing analyses.

is a Bcl-2 family member that acts in an antiapoptotic manner by interacting with Bax and Bak. Mst1 also phosphorylates Beclin1 at the endoplasmic reticulum (ER), thereby inhibiting autophagy during heart failure (3). Thus, Mst1, primarily localized in the cytosol at baseline, is translocated to other subcellular spaces in response to stress and phosphorylates distinct substrates, not necessarily limited to the Hippo signaling pathway, in a stimulus-specific manner. Although these results demonstrate the ability of Mst1 to phosphorylate downstream targets and modulate their functions, whether these substrates critically mediate the myocardial injury– or the heart failure–promoting effect of Mst1 remains to be elucidated.

We here report the generation of knockin (KI) mice with Bcl-xL that is not phosphorylatable by Mst1 (Bcl-xL S14A KI mice). Additionally, we show that a single mutation of Ser14 in Bcl-xL markedly attenuates myocardial injury in response to I/R and the development of DCM in response to persistent activation of Mst1, suggesting that Ser14 phosphorylation of endogenous Bcl-xL plays a critical role in mediating the effect of Mst1 upon both I/R injury and the development of DCM in vivo. Our results suggest the importance of the Mst1/Bcl-xL pathway, which is distinct from the canonical Hippo signaling pathway, in the context of treatment of cardiac disease.

Results

Generation and characterization of phosphorylation-resistant Bcl-xL S14A KI mice. To test the importance of Ser14 phosphorylation of endogenous Bcl-xL in the heart in vivo, we generated Bcl-xL S14A KI mice (Figure 1A). Homologous recombination in embryonic stem (ES) cells was confirmed by Southern blots and sequencing analyses (Supplemental Figure 1, A–C; supplemental material available online with this article; doi:10.1172/jci.insight.86217DS1). Chimeric male mice were then bred with C57BL/6J female mice for germline transmission. The neomycin cassette was deleted by crossing heterozygous KI (het KI) mice with CMV-Cre mice (Figure 1B). The mutation of Ser14 to Ala in mouse genomic DNA was confirmed by sequencing (Figure 1C).

Homozygous KI (homo KI) mice were viable and born at the predicted Mendelian ratio (Supplemental Table 1). Autopsy results at 11 to 12 weeks of age showed that whole body, heart, liver, and lung weights were not significantly different among WT, het KI, and homo KI mice (Supplemental Table 2). Histological assessment of the heart demonstrated no apparent sarcomere disarray, inflammatory cell infiltration, or interstitial fibrosis in homo KI mice (Supplemental Figure 2, A and B). Wheat germ agglutinin (WGA) staining indicated that the cross-sectional area of individual cardiomyocytes was also not significantly different among WT, het KI, and homo KI mice (Supplemental Figure 2C). The number of apoptotic myocytes, evaluated by TUNEL staining, was similar (Supplemental Figure 2D). In addition, the levels of Bcl-

xL, Bcl-2, Mst1, and active caspases in the heart (Supplemental Figure 2E) were similar among these mice, indicating that mechanisms of apoptosis may not be affected. Mitochondrial function was similar among WT, het KI, and homo KI mice, as evidenced by the absence of remarkable changes in mitochondrial basal oxygen consumption rates (Supplemental Figure 3A). Echocardiographic assessment showed that cardiac function was similar among WT, het KI, and homo KI mice (Supplemental Figure 3, B and C). Together, these data reveal that, despite the importance of both Hippo signaling and apoptosis during development, Ser14 phosphorylation of Bcl-xL is dispensable for embryonic and postnatal cardiac development, viability, and adult cardiac morphology. Furthermore, the lack of Ser14 phosphorylation of Bcl-xL does not affect mitochondrial and cardiac function in adult mice at baseline.

Inhibition of endogenous Bcl-xL Ser14 phosphorylation is protective against I/R. Mst1 is activated and phosphorylates Bcl-xL in the heart in response to I/R (4, 16, 17). We tested whether KI mice are protected against I/R injury in the heart (Supplemental Figure 4). After 30 minutes of ischemia and 30 minutes of reperfusion, Ser14 phosphorylation of Bcl-xL was substantially elevated in WT mice (Figure 2A). Increased Ser14 phosphorylation of Bcl-xL was accompanied by Mst1 activation, as evidenced by an increase in Mst1 phosphorylation at Thr183, and this was followed by increases in cleaved caspase-3 and -9, indicative of stimulation of apoptosis. In het KI mice, however, I/R-induced increases in Ser14 phosphorylation of Bcl-xL and activation of caspase-3 and -9 were significantly suppressed, whereas I/R-induced increases in Thr183 phosphorylation of Mst1 were unaffected (Figure 2A and Supplemental Figure 5A). Since I/R-induced increases in Ser14 phosphorylation of Bcl-xL were substantially suppressed, even in het KI mice, and the extent of the suppression was similar to that in transgenic mice with cardiac-specific overexpression of dominant-negative Mst1 (Tg-DN-Mst1 mice) (Figure 3A), we used het KI mice instead of homo KI mice for the rest of the I/R experiments. Bax translocates to mitochondria in response to oxidative stress and exposes an epitope consisting of amino acids 13 to 19 at the N-terminus of helix 1, which is detected by the monoclonal antibody 6A7 (18). The presence of detectable Bax 6A7 epitope correlates with cytochrome *c* release (19), and, thus, it is used as an indicator of Bax activation. Although we observed an increase in active Bax (6A7 epitope positive) in WT mice in response to I/R, this was suppressed in het KI mice (Figure 2, B and C). Increased oligomerization of Bax within the mitochondrial outer membrane promotes cytochrome *c* release into the cytosol (20). Consistent with the enhanced activation of Bax, cytochrome *c* release was increased in WT mice in response to I/R but was suppressed in het KI mice in comparison (Figure 2D and Supplemental Figure 5B). To examine the mechanism by which the Bcl-xL S14A mutant attenuates activation of Bax, we conducted immunoprecipitation assays. Both WT and het KI mice showed similar levels of interaction between Bax and Bcl-xL following sham operation. In response to I/R, WT mice showed only a slight increase in Bax–Bcl-xL interaction, despite Bcl-xL Ser14 phosphorylation, presumably due to the fact that more Bax translocates to mitochondria and that the total amount of the unphosphorylated form of Bcl-xL is also increased upon oxidative stress (21). In contrast, het KI mice exhibited a greater degree of interaction compared with WT mice (Supplemental Figure 5, C and D). These data suggest that the Mst1/Bcl-xL signaling pathway is critical for activation of the mitochondrial pathway of apoptosis through Bax. We further evaluated the Mst1/Lats2/YAP pathway, but there was no difference in phosphorylation of Lats2 (Thr1041) or YAP (Ser127) between WT and het KI mice in response to I/R (Figure 2, E and F), suggesting that inhibition of Bcl-xL phosphorylation does not affect the canonical Hippo signaling pathway. Furthermore, the presence of Bcl-xL (S14A) in het KI mice does not appear to act as a dominant negative for the Hippo signaling pathway.

Next, we assessed I/R-induced myocardial injury after 24-hour reperfusion. The area at risk (AAR) was similar in WT and het KI mice, suggesting that the gross architecture of the coronary circulation may not be affected in KI mice, and, thus, equal levels of myocardial ischemia were applied to WT and het KI mice (Figure 2G). However, the infarcted area/AAR was significantly smaller in het KI mice than in WT mice. In addition, there were significantly fewer apoptotic TUNEL-positive nuclei in KI mice than in WT mice (Figure 2H), suggesting that Ser14 phosphorylation of endogenous Bcl-xL plays an important role in mediating myocardial injury and cardiomyocyte apoptosis in response to I/R.

We have shown previously that suppression of endogenous Mst1 significantly attenuates I/R injury (1). In order to test whether the salutary effects of inhibiting Mst1 and inhibiting Ser14 phosphorylation of Bcl-xL are mediated through a common mechanism, we crossed het KI mice with Tg-DN-Mst1 mice (1). I/R increased Ser14 phosphorylation of Bcl-xL in WT mice, although the increase was suppressed to a similar degree among het KI, Tg-DN-Mst1, and het KI-Tg-DN-Mst1 mice (Figure 3A and Supplemental Figure 6).

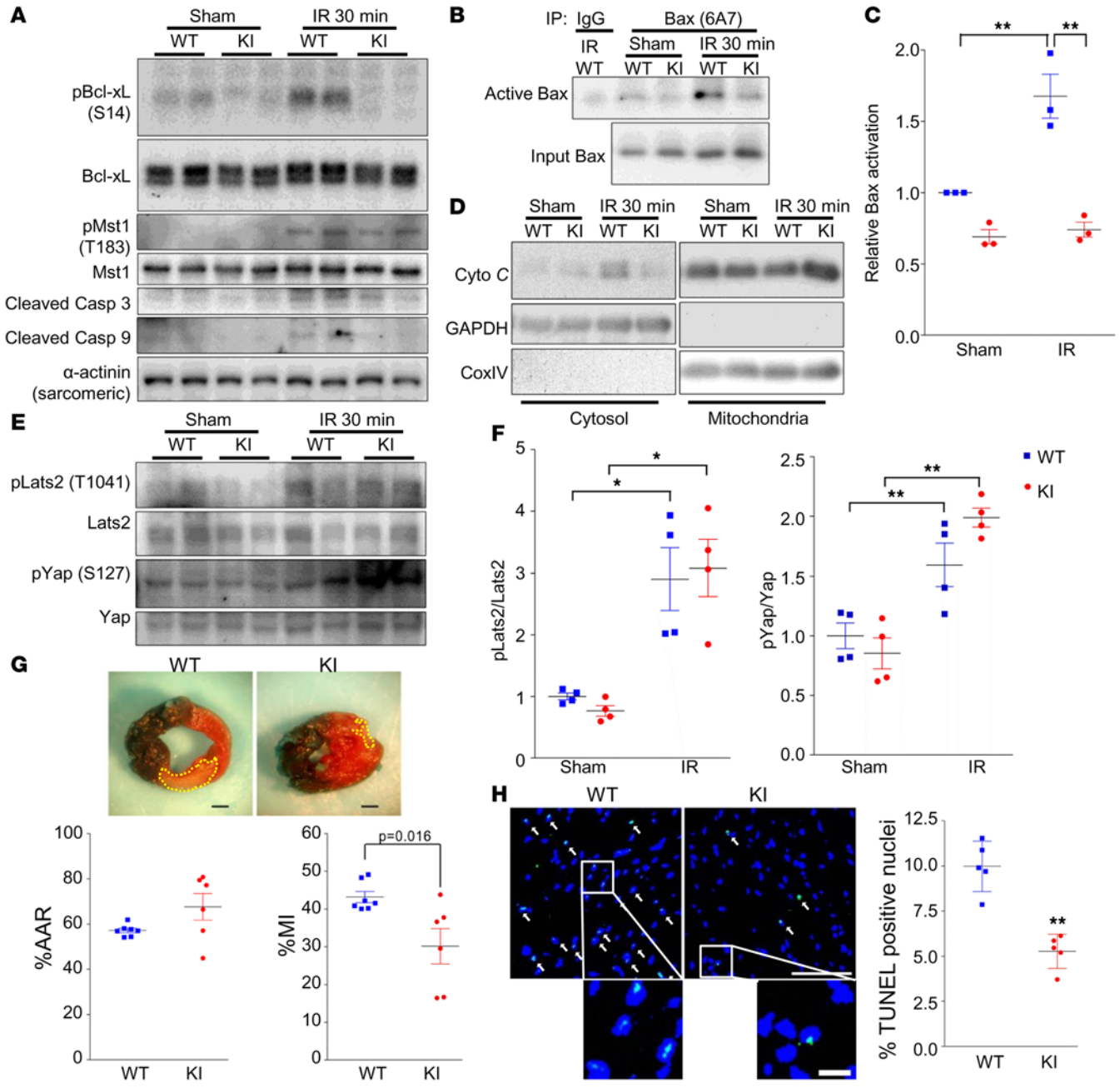

Figure 2. Bcl-xL S14A knockin mice are protected against ischemia/reperfusion injury. (**A**) Immunoblots showing expression of p-Bcl-xL (S14), total Bcl-xL, p-Mst1 (T183), total Mst1, and cleaved caspase-3 and -9 in the hearts of mice with sham operation or ischemia/reperfusion (I/R). (**B**) Immunoblots showing active Bax (6A7). The data are representative of 3 independent experiments. (**C**) Quantification of activated Bax (n = 3). (**D**) Immunoblots showing cytochrome c release in the hearts of WT and KI mice subjected to sham or I/R operation. The data are representative of 3 independent experiments. (**E**) Immunoblots showing p-Lats2 and p-YAP. (**F**) Quantification of the p-Lats2/Lats2 and p-YAP/YAP ratios (n = 4–6). The Hippo signaling pathway was not altered in KI mice compared with that in WT mice in response to sham or I/R operation. (**G**) Representative images of infarct size (white) and area at risk (AAR) (not blue) in the heart. Scale bar: 1 mm. Quantification of percentage AAR (AAR/left ventricle) and percentage myocardial infarction (MI; infarct area/AAR) (n = 6–7). (**H**) TUNEL-stained sections (ischemic area) of hearts from WT and KI mice following I/R and quantification of the percentage TUNEL-positive nuclei (n = 5). Scale bar: 50 μm (top); 10 μm (bottom). Data are mean ± SEM. *P < 0.01, **P < 0.001, 2-tailed unpaired Student's t test for 2 groups or 1-way ANOVA followed by the Newman-Keuls post-hoc analysis for 3 groups or more.

Het KI, Tg-DN-Mst1, and het KI-Tg-DN-Mst1 mice all displayed smaller infarcts and fewer TUNEL-positive nuclei when compared with those of WT mice in response to I/R, and they exhibited similar levels of protection (Figure 3, B–E). The lack of additional protection in the bigenic mice is consistent with the notion that the salutary effect of Mst1 inhibition against I/R injury is mediated primarily through suppression of Ser14 phosphorylation of Bcl-xL.

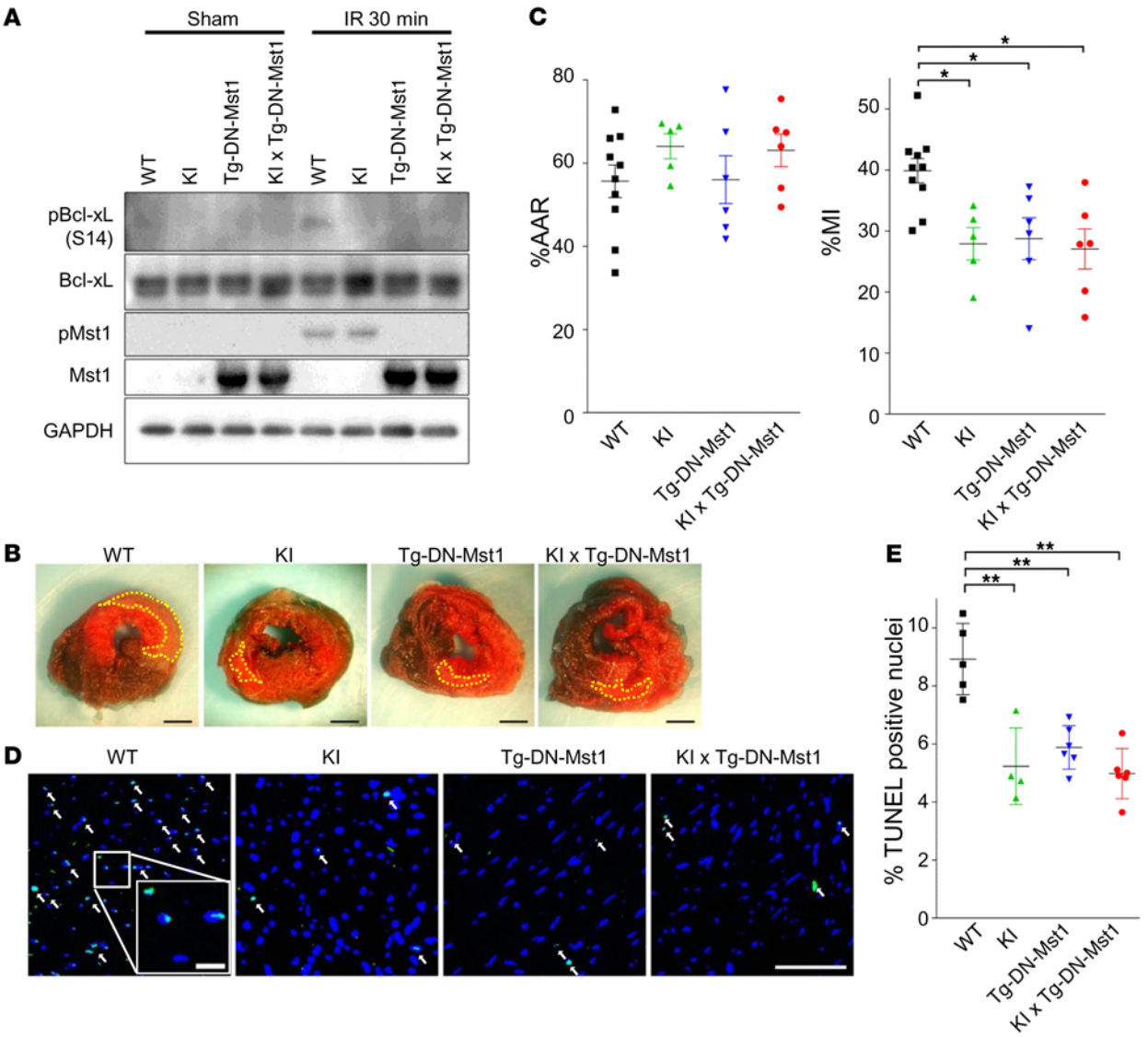

Figure 3. The protective effect of S14A knockin is part of the same pathway as that of Mst1 inhibition during ischemia/reperfusion. (**A**) Immunoblots showing p-Bcl-xL (S14) and total Bcl-xL. WT, Tg–dominant-negative–Mst1 (Tg-DN-Mst1), and bigenic mice generated by crossing knockin (KI) and Tg-DN-Mst1 mice (KI×Tg-DN-Mst1) were subjected to 30 minutes of ischemia and 30 minutes of reperfusion for protein expression analyses or 24 hours of reperfusion for measuring infarct size and TUNEL staining. (**B**) Representative images showing myocardial infarction (MI) and area at risk (AAR). White myocardium represents the infarct area. Scale bar: 1 mm. (**C**) Quantification of percentage AAR and percentage MI. Bigenic mice did not show additive protection against ischemia/reperfusion (I/R) compared with KI or Tg-DN-Mst1 mice (n = 5–10). (**D**) Representative TUNEL (green) and nuclear (blue) staining of the hearts (ischemic area) of the indicated mice following I/R. Scale bar: 50 μm; 10 μm (inset). (**E**) Quantification of TUNEL-positive nuclei (%) (n = 4–6). Data are mean ± SEM. *P < 0.05, **P < 0.001, 1-way ANOVA followed by the Newman-Keuls post-hoc analysis.

Suppression of Bcl-xL Ser14 phosphorylation attenuates Mst1-induced apoptosis and DCM. Overexpression of Mst1 in the heart is sufficient to induce DCM by promoting cell death (1). Upregulation of Mst1 also enhanced Ser14 phosphorylation of Bcl-xL in the heart (16). Therefore, we asked whether inhibition of Bcl-xL Ser14 phosphorylation normalizes Mst1-induced development of DCM. We crossed Tg-Mst1 mice with KI mice to generate het KI-Tg-Mst1 bigenic mice (Figure 4A). Since the KI mice were generated with the C57BL/6J background, we backcrossed Tg-Mst1 mice generated with the C57BL/6 background to the C57BL/6J background. Although the cardiac dysfunction observed in Tg-Mst1 mice with the C57BL/6J background was less severe than that in Tg-Mst1 mice with the C57BL/6 background (1), we confirmed that overexpression of Mst1 in the heart also induces DCM in the Tg-Mst1 mice backcrossed with the C57BL/6J background. Tg-Mst1 mice exhibited increased Ser14 phosphorylation of Bcl-xL, which was normalized in het KI-Tg-Mst1 bigenic mice (Supplemental Figure 7A).

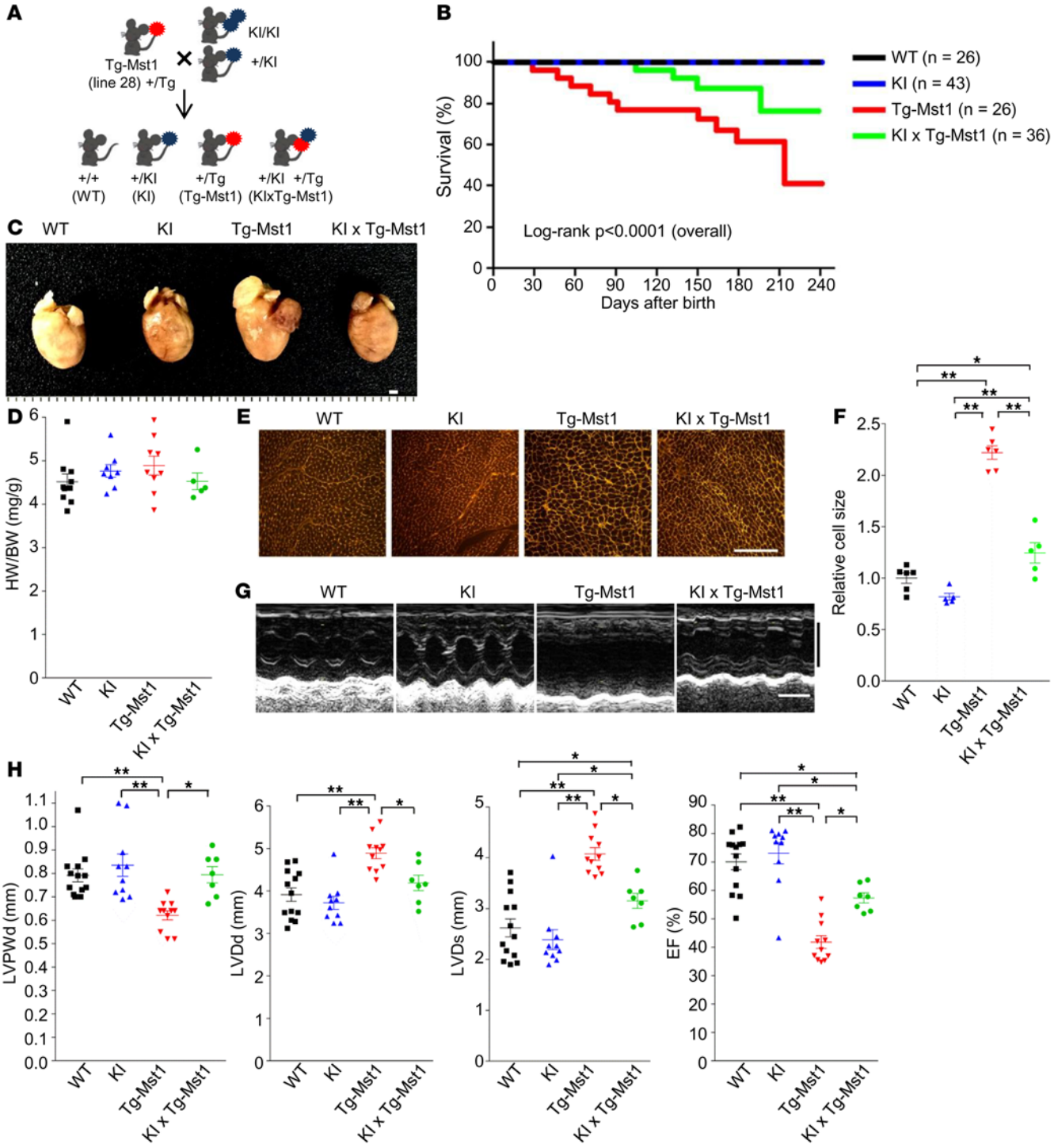

Figure 4. Inhibition of Bcl-xL Ser14 phosphorylation attenuates Mst1-induced cardiomyopathy. (**A**) Schematic representation of the breeding strategy for the study. Red circle represents Mst1 overexpression, and blue circle represents S14A. KI, knockin. (**B**) Kaplan-Meier survival analysis. (**C**) Gross appearance of the hearts obtained from the indicated 6-month-old mice. Scale bar: 1 mm. (**D**) Measurement of heart-weight-to-body-weight ratio (HW/BW). (**E**) Representative wheat germ agglutinin staining showing cardiomyocyte cell size. Scale bar: 100 μm. (**F**) Quantification of relative cell size (n = 5–6). (**G**) Representative images showing M-mode echocardiography. Transverse scale bar: 100 ms; vertical scale bar: 5 mm. (**H**) Echocardiographic analyses of cardiac morphology and function (n = 7–13). LVPWd, left ventricular (LV) posterior wall dimension at diastole; LVDd, LV end-diastolic dimension; LVDs, LV end-systolic dimension; EF, ejection fraction. Data are mean ± SEM. *P < 0.05, **P < 0.001, 1-way ANOVA followed by the Newman-Keuls post-hoc analysis.

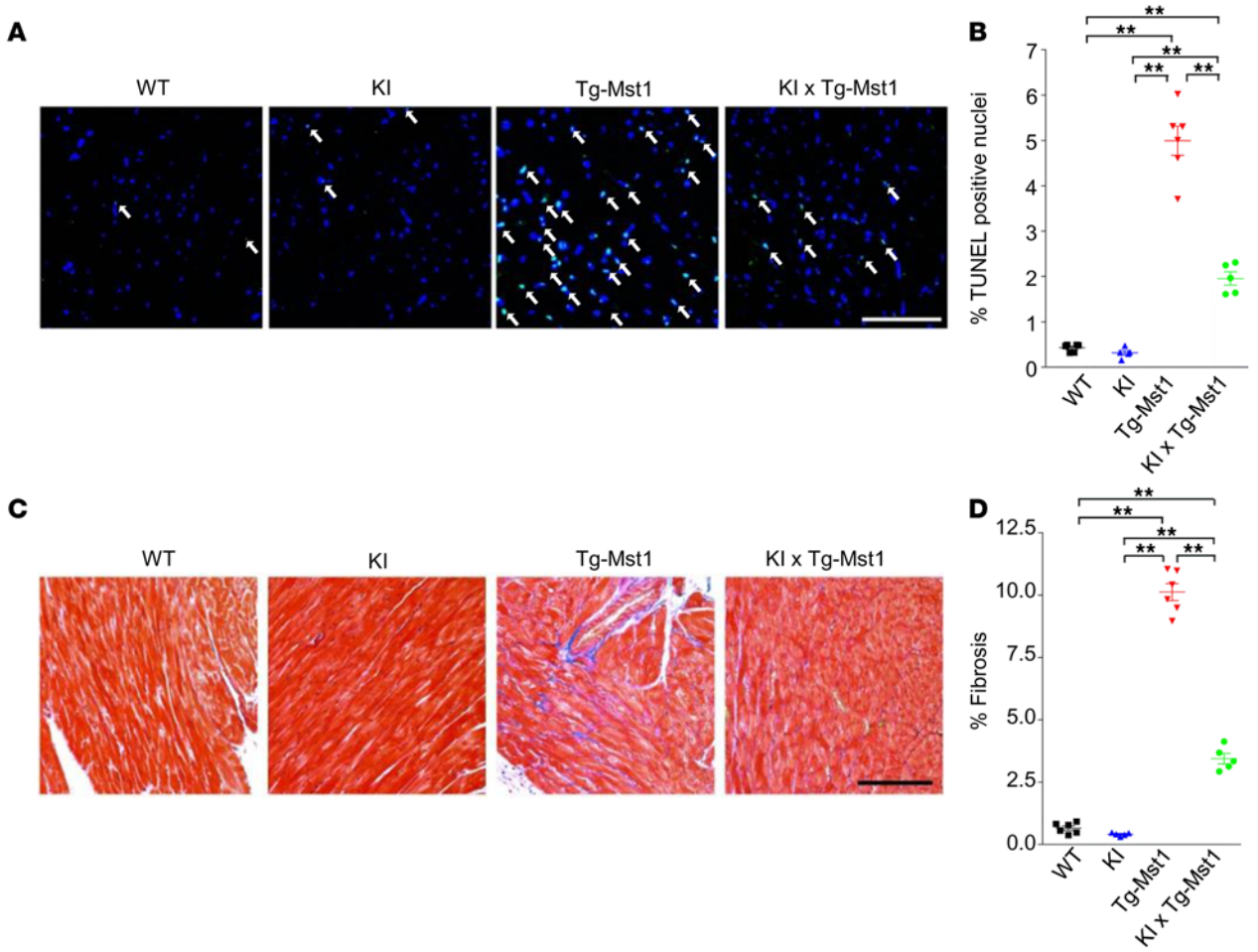

Figure 5. Inhibition of Bcl-xL Ser14 phosphorylation attenuates Mst1-induced cardiac dysfunction and apoptosis. (**A**) Representative TUNEL (green) and nuclear (blue) staining (scale bar: 50 μm). Arrows indicate TUNEL-positive nuclei. (**B**) Quantification of TUNEL-positive nuclei (%) (n = 5–6). (**C**) Representative heart sections stained with Masson's trichrome (scale bar: 100 μm). (**D**) Quantification of percentage fibrosis (n = 5–6). Data are mean ± SEM. $^{**}P <$ 0.001, 1-way ANOVA followed by the Newman-Keuls post-hoc analysis.

Tg-Mst1 mice exhibited early mortality beginning at 4 weeks of age (Figure 4B). However, het KI-Tg-Mst1 bigenic mice exhibited a significantly lower mortality rate than Tg-Mst1 mice (log-rank $P = 0.0286$ between the 2 groups). The gross morphology of WT and het KI mouse hearts at 6 months of age was indistinguishable. In contrast, Tg-Mst1 mouse hearts exhibited dilatation of all 4 chambers (Figure 4C), disorganized cardiomyocytes, and reduced wall thickness (Supplemental Figure 7B), all of which were partially reversed in het KI-Tg-Mst1 mice (Figure 4C and Supplemental Figure 7B). Despite the enlargement of the heart in Tg-Mst1 mice, the heart-weight-to-body-weight ratios in Tg-Mst1 mice were comparable to those in WT mice (Figure 4D). Histological assessment of cardiomyocyte cross-sectional area with WGA staining indicated, however, that individual cardiomyocytes underwent hypertrophy in Tg-Mst1 mice, while this was largely, if not completely, reversed in the bigenic mice (Figure 4, E and F). The upregulation of β-myosin heavy chain (βMHC) observed in Tg-Mst1 mice was significantly attenuated in het KI-Tg-Mst1 mice, but that of other fetal-type genes, including atrial natriuretic factor (ANF) and brain natriuretic peptide (BNP), was not significantly blunted in het KI-Tg-Mst1 mice (Supplemental Figure 7C). Echocardiographic assessment indicated that left ventricular (LV) chamber size and function were normal in WT and het KI mice at 6 months of age (Figure 4, G and H). In contrast, significant increases in LV end-diastolic and end-systolic dimensions and significant decreases in LV wall thickness and systolic function were observed in Tg-Mst1 mice, but the changes in these parameters were significantly reversed in het KI-Tg-Mst1 bigenic mice (Figure 4, G and H). These findings suggest that phosphorylation of endogenous Bcl-xL at Ser14 plays an important role in the development of Mst1-induced cardiomyopathy. Histological analyses indicated that there is a marked increase in the number of TUNEL-positive myocytes in Tg-Mst1 mice but that the number of TUNEL-positive myocytes was sub-

stantially smaller in bigenic mice (Figure 5, A and B). Tg-Mst1 mice also exhibited a significant increase in LV interstitial fibrosis, as evaluated with Masson's trichrome staining, compared with that in control mice, whereas het KI-Tg-Mst1 bigenic mice exhibited less fibrosis than Tg-Mst1 mice (Figure 5, C and D). Together, these data suggest that inhibition of Ser14 phosphorylation of Bcl-xL attenuates Mst1-induced increases in myocardial apoptosis, fibrosis, and the development of cardiomyopathy.

To examine whether this protective role is mediated through the mitochondrial pathway of apoptosis, we performed immunoprecipitation assays using Bcl-xL. Both WT and het KI mice exhibited similar levels of interaction between Bax and Bcl-xL, possibly due to the fact that Ser14 phosphorylation of Bcl-xL in WT mice is negligible at baseline. Although Tg-Mst1 mice showed a significant reduction in the binding of Bcl-xL to Bax, het KI-Tg-Mst1 bigenic mice showed only a modest reduction (Supplemental Figure 8, A and B). Consistent with this result, activation of Bax was significantly increased in Tg-Mst1 mice, whereas the Mst1-induced increase in active Bax was attenuated in the bigenic mice (Supplemental Figure 8, C and D).

We have shown previously that Mst1 phosphorylates Beclin1 at Thr108, which inhibits autophagy and induces apoptosis by stimulating an interaction between Beclin1 and Bcl-2/Bcl-xL (3). Since the presence of unphosphorylatable Bcl-xL may increase the availability of Mst1 for phosphorylation of other substrates, we examined whether the phosphorylation status of Beclin1 and autophagy are affected in het KI mice. As reported previously, Tg-Mst1 mice showed increased phosphorylation of Beclin1 (Thr108), accompanied by suppression of autophagy, as evidenced by increases in p62. However, phosphorylation of Beclin1 (Thr108) and suppression of autophagy remained unchanged in het KI-Tg-Mst1 bigenic mice (Supplemental Figure 9). We further tested whether Mst1-induced apoptosis is mediated through the phosphorylation of Bcl-xL and Beclin1 pathways in an independent manner. Rat neonatal cardiomyocytes were transduced with adenovirus (Ad) harboring Mst1 (Ad-Mst1), together with either Ad-Bcl-xL-WT or S14A and/or either Ad-Beclin1-WT or T108A for 48 hours. Cleaved caspase-3 expression and TUNEL-positive nuclei were markedly attenuated by expression of either Bcl-xL-S14A or Beclin1-T108A compared with that in cardiomyocytes expressing either Bcl-xL-WT or Beclin1-WT (Supplemental Figure 10, A and B). Furthermore, simultaneous application of Bcl-xL-S14A and Beclin1-T108A further suppressed Mst1-induced increases in TUNEL-positive cardiomyocytes, indicating that Bcl-xL-S14A and Beclin1-T108A have additive effects. These results indicate that Mst1-induced apoptosis is independently regulated by phosphorylation of Bcl-xL and that of Beclin1 (Supplemental Figure 11).

Discussion

Mst1 is an upstream central regulator of the Hippo signaling pathway that inhibits cell proliferation and promotes apoptosis through phosphorylation of Lats1/2, thereby regulating organ size, differentiation, and regeneration (7–10). Mst1 also regulates other substrates that do not belong to the canonical Hippo signaling pathway, including Beclin1 and Bcl-xL, thereby regulating a wide variety of cellular functions, including autophagy and mitochondrial mechanisms of apoptosis. Thus, it is important to assess the role of endogenous substrates of Mst1 in order to better understand the function of Mst1 in response to a given stress. Here, we demonstrate that Ser14 phosphorylation of endogenous Bcl-xL plays an important role in mediating the effect of Mst1 upon I/R injury and the development of heart failure. Our results suggest the importance of the Mst1/Bcl-xL noncanonical Hippo signaling pathway localized in mitochondria as a therapeutic target for cardiac disease, including reperfusion injury and DCM.

Mst1 is activated in the heart in response to many different types of stresses, including I/R and pressure and volume overload, through a wide variety of molecular mechanisms involving oxidative stress, mechanical stress, and cytokines. Mst1 is localized primarily in the cytosol at baseline but can be translocated to the nucleus, mitochondria, and the ER and activated by distinct mechanisms involving assembly by scaffolding proteins, such as Rassf1A and NF2. In particular, I/R and oxidative stress cause Mst1 in cardiomyocytes to be translocated to mitochondria and activated through K-Ras and Rassf1A-dependent mechanisms. The activated Mst1 then phosphorylates Bcl-xL at Ser14 (16). Although we have shown that Ser14 phosphorylation of Bcl-xL dissociates Bcl-xL from Bax, thereby activating Bax and inducing the mitochondrial pathway of apoptosis (16), it is possible that Mst1 has additional substrates in mitochondria that may play more important roles in mediating the effect of Mst1. Furthermore, given that Mst1 also participates in signaling cascades in other subcellular compartments, including the canonical signaling pathway, the relative importance of Ser14 phosphorylation of endogenous Bcl-xL has been unclear. We here show that a lack of Ser14 phosphorylation of Bcl-xL markedly attenuates I/R injury and

the development of cardiomyopathy in Tg-Mst1 mice in vivo. Since Ser14 phosphorylation of Bcl-xL is completely abrogated in the absence of Mst1 (16), our results strongly suggest that Ser14 phosphorylation of Bcl-xL critically mediates the function of Mst1 in response to I/R. The fact that het KI mice and Tg-DN-Mst1 mice exhibited almost equal levels of protection and the fact that het KI-Tg-DN-Mst1 mice failed to show significant additive protection suggest that Ser14 phosphorylation of Bcl-xL is the key mechanism mediating the proapoptotic effect of Mst1 during I/R injury.

We have shown previously that Mst1 phosphorylates Beclin1 at the ER (3). Mst1 phosphorylates Thr108 located in the BH3 domain of Beclin1 and enhances the interaction between the BH3 domain of Beclin1 and Bcl-2/Bcl-xL and dissociation of Bcl-2/Bcl-xL from Bax. This mechanism would not necessarily produce an additive effect upon Bax-mediated cell death, which we presume should take place when Ser14 phosphorylation of Bcl-xL is inhibited, and it is possible that this mechanism may also participate in Mst1-induced cell death. If so, it is interesting that multiple mechanisms mediating Mst1-induced cell death converge at the level of Bax through phosphorylation of Bcl-2–related proteins. Although we showed that Mst1-induced apoptosis is independently regulated by phosphorylation of Bcl-xL and that of Beclin1 in cardiomyocytes with an adenovirus-mediated overexpression model in vitro, at present, it remains unknown whether a given stress has redundant mechanisms to activate Bax or uses a specific pathway localized at different subcellular locations, depending upon the nature of stress.

It has been suggested that there may be functional redundancy in the antiapoptotic functions of Bcl-2 and Bcl-xL. However, given that het KI mice were protected from myocardial I/R injury and Mst1-induced DCM and that Ser14 of Bcl-xL in the BH4 domain is not conserved in Bcl-2, we believe that the Mst1/Bcl-xL pathway has a nonredundant function and acts as one of the primary mechanisms regulating pathologic cell death in the heart.

Ser14 phosphorylation of Bcl-xL was increased in response to stresses, such as I/R and heart failure in the heart. We have shown previously that Bcl-xL Ser14 phosphorylation is primarily mediated by Mst1. Interestingly, Ser14 phosphorylation was largely suppressed in het KI mice in response to I/R and overexpression of Mst1. Since Thr183 phosphorylation of Mst1, Thr1041 phosphorylation of Lats2, and Ser127 phosphorylation of YAP were not affected, it is unlikely that the presence of S14A Bcl-xL globally affects Mst1 or the Hippo pathway. The mechanism by which het KI is sufficient to substantially downregulate stress-induced Ser14 phosphorylation of Bcl-xL remains to be elucidated. It is possible that a threshold level of substrate is needed to initiate and feedforward the enzymatic reaction of phosphorylation by Mst1, which is translocated from the cytosol to mitochondria when it is activated by I/R in cardiomyocytes.

Suppression of Ser14 phosphorylation of Bcl-xL markedly attenuated the development of DCM in Tg-Mst1 mice. This suggests that Ser14 of Bcl-xL is an important substrate of Mst1 in the heart, and, since Mst1 is activated by many clinically relevant cardiac stresses, such as pressure overload, myocardial infarction, and heart failure, Ser14 phosphorylation of Bcl-xL may be an important target for treatment of heart disease. Nevertheless, although suppression of Ser14 phosphorylation of Bcl-xL suppressed I/R injury as effectively as suppression of endogenous Mst1 activity, it did not fully prevent the development of DCM in Tg-Mst1 mice. Since Ser14 phosphorylation of Bcl-xL was almost fully suppressed in het KI-Tg-Mst1 mice, the incomplete rescue of DCM is unlikely to be due to incomplete suppression of Ser14 phosphorylation of Bcl-xL. We speculated that other substrates of Mst1, such as Lats2, a component of the canonical Hippo pathway, also play an important role in mediating the development of DCM in Tg-Mst1 mice. In addition, we have shown previously that Mst1 phosphorylates Beclin1 at the ER, thereby inhibiting autophagy. Suppression of autophagy exacerbates heart failure by stimulating accumulation of damaged mitochondria and misfolded proteins (22). Furthermore, we recently observed that Mst1 and the downstream Hippo pathway are activated by NF2-dependent mechanisms in the nucleus (T. Matsuda et al., unpublished observations). Thus, substrates of Mst1 in other subcellular compartments may also participate in the development of heart failure when Mst1 is globally activated in Tg-Mst1 mice.

In summary, we demonstrate that Ser14 of endogenous Bcl-xL is a critical substrate of Mst1 and that it functionally plays an essential role in mediating the effect of Mst1 upon I/R injury and the development of DCM. Our study also suggests the importance of the noncanonical Hippo signaling pathway in mitochondria. Ser14 phosphorylation of Bcl-xL may be an important therapeutic target for treatment of ischemic heart diseases and heart failure.

Methods

Generation of gene-targeted mice. Bcl-xL genomic DNA was isolated from the BAC clone (RP23-106A3) to construct the Bcl-xL S14A KI targeting vector. PCR-based site-directed mutagenesis was performed to introduce a single mutation of T to G in codon 14 in exon 2 of Bcl-xL to change codon 14 from Ser to Ala. A pGK neo cassette flanked by two lox P sites was inserted into intron 2 for selection of the targeted allele such that it could subsequently be deleted by Cre-mediated recombination. The DNA sequences of exons 1 and 2 and PCR fragments used for constructing the targeting vector were confirmed by DNA sequencing. The targeting vectors were linearized with *PmeI* and subsequently electroporated into R1 ES cells. G418-resistant ES clones were screened for homologous recombination by *MfeI* digestion, followed by Southern blot analysis. Briefly, genomic DNA was extracted from G418-resistant ES cell clones, which was followed by *MfeI* digestion, separation on a 0.8% agarose gel, and blotting onto a positively charged nylon transfer membrane (GE Healthcare). The DNA probes, 492-bp (for a 5′ probe) and 496-bp (for a 3′ probe) DNA fragments, were isolated from the BAC clone and subcloned into the pBluescript vector using the following primers: forward, 5′-ATGAATTCCTGCTCGTACACTGATAATTGG-3′, and reverse, 5′-ATGGTACCCTGAGTGTTCTTGCTGGGATT-3′ for a 5′ probe, and forward, 5′-ATGAATTCGCCTCTGGCCATACTACTGC-3′ and, reverse, 5′-ATTGGTACCTGCACTGAAGAAGCCACAAC-3′ for a 3′ probe. The fragment was isolated from the pBluescript plasmid with *EcoRI* and *KpnI* digestion to generate the DNA probes and subsequently radiolabeled using [^{32}P] dCTP by random priming (Roche), followed by radiolabeled DNA purification (Roche). DNA blots were hybridized with the radiolabeled probe and visualized by autoradiography. Three independent homologous recombinant ES clones were microinjected into blastocysts from C57BL/6J mice and transferred into pseudopregnant recipients to generate male chimeras. The chimeric male mice resulting from the microinjection were bred with C57BL/6J female mice to generate germline-transmitted heterozygous S14A KI mice. PCR analysis was performed on tail DNA from offspring from the intercrosses using standard procedures. Sequence analysis was performed on PCR products to verify the presence of the mutations using standard procedures. To avoid interference of the pGK neo cassette with expression of the mutant alleles, the neomycin cassette was deleted by crossing het KI mice with CMV-Cre mice (Jackson Laboratory). The mutant offspring were backcrossed into the C57BL/6J background.

Animal experiments. Tg-Mst1 and Tg-DN-Mst1 mice have been described previously (1). CMV-Cre and C57BL/6J mice were obtained from the Jackson Laboratory. KI mice and Tg-Mst1 or Tg-DN-Mst1 mice were bred to generate bigenic mice. Mice were housed in a temperature-controlled environment, with 12-hour light/dark cycles, in which they received food and water ad libitum. The myocardial I/R study was performed as described previously (16). In brief, 2- to 3-month-old male mice were anesthetized by intraperitoneal injection of pentobarbital sodium (50 mg/kg). A rodent ventilator (model 683; Harvard Apparatus Inc.) was used with 65% oxygen. The animals were kept warm with heat lamps. Rectal temperature was monitored and maintained at between 36°C and 37°C. The chest was opened by a horizontal incision at the third intercostal space. I/R was achieved by ligating the anterior descending branch of the left coronary artery with an 8-0 Prolene suture, with silicon tubing (1-mm outer diameter) placed on top of the left anterior descending coronary artery (LAD), 2 mm below the border between the left atrium and the LV. Ischemia was confirmed by ECG change. After occlusion for 30 minutes, the silicon tubing was removed to achieve reperfusion, and the rib space and overlying muscles were closed. When recovered from anesthesia, the mice were extubated and returned to their cages. The duration of reperfusion was 30 minutes or 24 hours for protein expression analyses and 24 hours for measurement of infarct size and histological analyses. Mice were housed in a climate-controlled environment.

Measurement of infarct size. Twenty-four hours after reperfusion, mice were anesthetized and the chest was opened. After reocclusion of the LAD with the same suture, the ascending aorta was cannulated and 1% Alcian blue dye was perfused into the aorta and coronary arteries to demarcate the ischemic AAR. Hearts were excised and LVs were sliced into 1-mm-thick cross sections. The heart sections were then incubated with a 1% triphenyltetrazolium chloride solution at 37°C for 10 minutes. The infarct area (pale), the AAR (not blue), and the total LV area from both sides of each section were measured using ImageJ, and the values obtained were averaged. The percentage of area of infarction and the percentage of AAR of each section were multiplied by the weight of the section and then totaled for all sections. AAR/LV and infarct area/AAR were expressed as percentages.

Isolation of rat neonatal cardiomyocytes. Primary cultures of ventricular cardiomyocytes were prepared from 1-day-old Charles River Laboratories/Wistar Institute BR-Wistar rats (Harlan Laboratories) as described previously (23).

Adenovirus construct. Generation of recombinant adenovirus vectors for overexpression was described previously (3, 16).

Immunoprecipitation and immunoblotting. Heart homogenates were prepared in RIPA buffer containing protease and phosphatase inhibitors (Sigma-Aldrich). Samples were incubated with anti-Bcl-xL (54H6) antibody (Cell Signaling) overnight at 4°C, and immunocomplexes were precipitated following 1 hour of incubation with sepharose A/G beads (Santa Cruz). After immunoprecipitation, the samples were washed with lysis buffer 5 times, and the beads were boiled in 30-μl Laemmli sample buffer, followed by SDS-PAGE, and immunoblotting. Electrophoresis, electrotransfer, and immunoblotting were performed as described previously (3). For immunoblot analysis, the following antibodies were used: p-Mst1/2 (T183/180) (product 3681), Bcl-xL (product 2764), Bcl-2 (product 2876), Bax (product 2772), cleaved caspase-3 (product 9661), cleaved caspase-9 (product 7237), cytochrome *c* (product 11940), YAP, p-YAP (S127), Cox IV, GAPDH (14C10), and secondary antibodies (anti-mouse or rabbit IgG) conjugated with horseradish peroxidase (Cell Signaling Technology); Mst1 (BD Transduction Labs 611052); active Bax (6A7 epitope Calbiochem); p-Lats2 (gift of Hiroshi Nojima, Osaka University, Osaka, Japan); Lats2 (Santa Cruz SAB4501146); and α-actinin (sarcomeric) (Sigma-Aldrich A7811). p-Bcl-xL (S14) was generated as described previously (16). Densitometry was performed using ImageJ software.

Detection of the active form of Bax. Heart were lysed in 200 μl of CHAPS buffer (150 mmol/l NaCl and 10 mmol/l HEPES [pH 7.4]) containing protease and phosphatase inhibitors (Sigma-Aldrich) to prevent conformational activation of Bax (24). Samples were incubated with primary antibody overnight at 4°C, and immunocomplexes were precipitated following 1 hour of incubation with sepharose A/G beads (Santa Cruz). After extensive washing with CHAPS buffer, beads were boiled in 30 μl Laemmli sample buffer, followed by SDS-PAGE and immunoblot with anti-Bax antibody (Cell Signaling Technology).

Subcellular fractionation. Isolated mouse ventricles were homogenized and fractionated as described previously (25). Briefly, homogenates were prepared in ice-cold Buffer A (200 mmol/l mannitol, 50 mmol/l sucrose, 10 mmol/l KCl, 1 mmol/l EDTA, 10 mmol/l HEPES-KOH [pH 7.4], 0.1% BSA, 0.1 mmol/l Na_3VO_4, 5 μg/ml aprotinin, and 5 μg/ml leupeptin) and centrifuged at 600 *g* for 5 minutes at 4°C. Supernatants were then centrifuged at 3,500 *g* for 15 minutes at 4°C. The resultant supernatant was centrifuged at 100,000 *g* for 2 hours to separate cytosol and microsome/sarcoplasmic reticulum fractions. The pellet was resuspended in Buffer A and centrifuged at 1,500 *g* for 5 minutes. The resulting supernatant was centrifuged at 10,000 *g* for 20 minutes at 4°C, and then the pellet, representing the mitochondria-enriched fraction, was resuspended in Buffer A.

Histological analyses. Histological analyses were performed as described previously (3). In brief, heart samples were fixed in 4% paraformaldehyde, embedded in paraffin, and sectioned at 6-μm thickness. H&E staining and Masson's trichrome staining were performed following standard procedures. Interstitial fibrosis was evaluated by Masson's trichrome staining. The myocyte cross-sectional area was measured from images captured from WGA-stained sections. The outlines of cardiomyocytes were traced in each section using ImageJ software.

Evaluation of apoptosis. DNA fragmentation was detected with the use of TUNEL, as described previously (1). Nuclear density was determined by manual counting of DAPI-stained nuclei in 5 to 8 fields for each sample, and the number of TUNEL-positive nuclei was counted by examining the same fields. We evaluated apoptotic cell numbers in the ischemic area 24 hours after reperfusion and in the midportion of the LV at baseline.

TUNEL staining in cultured cardiomyocytes. Cardiomyocytes were fixed in PBS containing 4% paraformaldehyde. Staining was performed using the In Situ Cell Death Detection Kit (Roche) according to the manufacture's instruction.

Echocardiography. Echocardiography was performed as described previously (3). Briefly, mice were anesthetized using avertin (Sigma-Aldrich) and were subjected to 2-dimension–guided M-mode measurements of LV internal diameter to measure systolic function. LV end-diastolic dimension (LVDd) was measured at the time of the apparent maximal LV diastolic dimension, and LV end-systolic dimension (LVDs) was measured at the time of the most anterior systolic excursion of the posterior wall. LV ejection fraction (LVEF) was calculated using the following formula: $LVEF\ (\%) = 100 \times (LVDd^3 - LVDs^3)/LVDd^3$.

Mitochondrial analyses using the Seahorse system. The basal oxygen consumption rate in isolated mitochondria from mouse hearts was measured by a Seahorse XF24 Extracellular Flux Analyzer (Seahorse Bioscience) as described previously (26). Briefly, the mitochondrial fraction of mouse hearts was prepared

for measurements of basal oxygen consumption rate as described above. To minimize variability between wells, mitochondria were first diluted 10 times in cold 1× MAS (70 mmol/l sucrose, 220 mmol/l mannitol, 10 mmol/l KH_2PO_4, 5 mmol/l $MgCl_2$, 2 mmol/l HEPES, 1.0 mmol/l EGTA, and 0.2% (w/v) fatty acid–free BSA, pH 7.2 at 37°C) with substrate (0.5 mol/l succinate, 0.5 mol/l malate, and 0.5 mol/l pyruvate) and then subsequently diluted to the concentration required for plating. Next, 50 μl of mitochondrial suspension was delivered to each well (except for background correction wells) while the plate was on ice. The plate was then transferred to a centrifuge equipped with a swinging bucket microplate adaptor and spun at 1,500 *g* for 30 minutes at 4°C. After centrifugation, 450 μl of 1× MAS with substrate was added to each well. The mitochondria were viewed briefly under a microscope at ×20 to ensure consistent adherence to the well and then incubated at 37°C for 8 to 10 minutes to allow the plate to warm. The plate was then transferred to the XF24 Analyzer and the experiment initiated.

Quantitative PCR. Total RNA was extracted from mouse hearts using TRIzol reagent (Invitrogen). Reverse transcription and quantitative PCR were performed as previously described (27). Relative mRNA expression was determined by the ΔΔ-Ct method normalized to ribosomal RNA (18S) level. The following oligonucleotide primers were used in this study: ANF, sense 5′-ATGGGCTCCTTCTCCATCAC-3′ and antisense 5′-ATCTTCGGTACCGGAAGCTG-3′; BNP, sense 5′-AAGTCCTAGCCAGTCTCCAGA-3′ and antisense 5′-GAGCTGTCTCTGGGCCATTTC-3′; βMHC, sense 5′-GCCAACACCAACCTGTCCAAGTTC-3′ and antisense 5′-TGCAAAGGCTCCAGGTCTGAGGGC-3′; and 18S rRNA, sense 5′-CGCGGTTCTATTTTGTTGGT-3′ and antisense 5′-AGTCGGCATCGTTTATGGTC-3′.

Statistics. All values are expressed as mean ± SEM. Statistical analyses were carried out by 2-tailed unpaired Student's *t* test for 2 groups or 1-way ANOVA followed by the Newman-Keuls post-hoc analysis for 3 groups or more. Survival curves were plotted by the Kaplan-Meier method, with statistical significance analyzed by log-rank test. A *P* value of less than 0.05 was considered significant. Statistical analyses were performed using GraphPad Prism (GraphPad Software).

Study approval. All protocols concerning the use of animals were approved by the Institutional Animal Care and Use Committee at Rutgers New Jersey Medical School.

Author contributions

MN designed and performed experiments, analyzed data, and wrote the manuscript. PZ performed animal surgery. DPDR and YM performed experiments and analyzed data. JS designed the studies, analyzed the data, and wrote the manuscript.

Acknowledgments

We thank Daniela Zablocki for critical reading of the manuscript. This work was supported in part by US Public Health Service grants HL67724, HL91469, HL102738, HL112330, and AG23039 (to J. Sadoshima). This work was also supported by the Leducq Fondation Transatlantic Network of Excellence (to J. Sadoshima) and American Heart Association Founders Affiliate Postdoctoral Fellowship 14POST18870094 (to M. Nakamura).

Address correspondence to: Junichi Sadoshima, Department of Cell Biology and Molecular Medicine, Cardiovascular Research Institute, Rutgers New Jersey Medical School, 185 South Orange Ave., MSB G-609, Newark, New Jersey 07103, USA. Phone: 973.972.8619; E-mail: sadoshju@njms.rutgers.edu.

1. Yamamoto S, et al. Activation of Mst1 causes dilated cardiomyopathy by stimulating apoptosis without compensatory ventricular myocyte hypertrophy. *J Clin Invest*. 2003;111(10):1463–1474.
2. Chen SN, Gurha P, Lombardi R, Ruggiero A, Willerson JT, Marian AJ. The hippo pathway is activated and is a causal mechanism for adipogenesis in arrhythmogenic cardiomyopathy. *Circ Res*. 2014;114(3):454–468.
3. Maejima Y, et al. Mst1 inhibits autophagy by promoting the interaction between Beclin1 and Bcl-2. *Nat Med*. 2013;19(11):1478–1488.
4. Odashima M, et al. Inhibition of endogenous Mst1 prevents apoptosis and cardiac dysfunction without affecting cardiac hypertrophy after myocardial infarction. *Circ Res*. 2007;100(9):1344–1352.
5. Del Re DP, et al. Proapoptotic Rassf1A/Mst1 signaling in cardiac fibroblasts is protective against pressure overload in mice. *J Clin Invest*. 2010;120(10):3555–3567.
6. Pan D. The hippo signaling pathway in development and cancer. *Dev Cell*. 2010;19(4):491–505.
7. Matallanas D, Romano D, Hamilton G, Kolch W, O'Neill E. A Hippo in the ointment: MST signalling beyond the fly. *Cell Cycle*. 2008;7(7):879–884.

8. Wackerhage H, Del Re DP, Judson RN, Sudol M, Sadoshima J. The Hippo signal transduction network in skeletal and cardiac muscle. *Sci Signal*. 2014;7(337):re4.
9. Heallen T, et al. Hippo pathway inhibits Wnt signaling to restrain cardiomyocyte proliferation and heart size. *Science*. 2011;332(6028):458–461.
10. Song H, et al. Mammalian Mst1 and Mst2 kinases play essential roles in organ size control and tumor suppression. *Proc Natl Acad Sci U S A*. 2010;107(4):1431–1436.
11. Yu FX, Zhao B, Guan KL. Hippo pathway in organ size control, tissue homeostasis, and cancer. *Cell*. 2015;163(4):811–828.
12. Callus BA, Verhagen AM, Vaux DL. Association of mammalian sterile twenty kinases, Mst1 and Mst2, with hSalvador via C-terminal coiled-coil domains, leads to its stabilization and phosphorylation. *FEBS J*. 2006;273(18):4264–4276.
13. Chan EH, Nousiainen M, Chalamalasetty RB, Schafer A, Nigg EA, Sillje HH. The Ste20-like kinase Mst2 activates the human large tumor suppressor kinase Lats1. *Oncogene*. 2005;24(12):2076–2086.
14. Praskova M, Xia F, Avruch J. MOBKL1A/MOBKL1B phosphorylation by MST1 and MST2 inhibits cell proliferation. *Curr Biol*. 2008;18(5):311–321.
15. McPherson JP, et al. Lats2/Kpm is required for embryonic development, proliferation control and genomic integrity. *EMBO J*. 2004;23(18):3677–3688.
16. Del Re DP, et al. Mst1 promotes cardiac myocyte apoptosis through phosphorylation and inhibition of Bcl-xL. *Mol Cell*. 2014;54(4):639–650.
17. Shao D, et al. A functional interaction between Hippo-YAP signalling and FoxO1 mediates the oxidative stress response. *Nat Commun*. 2014;5:3315.
18. Hsu YT, Youle RJ. Bax in murine thymus is a soluble monomeric protein that displays differential detergent-induced conformations. *J Biol Chem*. 1998;273(17):10777–10783.
19. Nechushtan A, Smith CL, Hsu YT, Youle RJ. Conformation of the Bax C-terminus regulates subcellular location and cell death. *EMBO J*. 1999;18(9):2330–2341.
20. Czabotar PE, Lessene G, Strasser A, Adams JM. Control of apoptosis by the BCL-2 protein family: implications for physiology and therapy. *Nat Rev Mol Cell Biol*. 2014;15(1):49–63.
21. von Harsdorf R, Li PF, Dietz R. Signaling pathways in reactive oxygen species-induced cardiomyocyte apoptosis. *Circulation*. 1999;99(22):2934–2941.
22. Maejima Y, Chen Y, Isobe M, Gustafsson AB, Kitsis RN, Sadoshima J. Recent progress in research on molecular mechanisms of autophagy in the heart. *Am J Physiol Heart Circ Physiol*. 2015;308(4):H259–H268.
23. Sadoshima J, Izumo S. Molecular characterization of angiotensin II — induced hypertrophy of cardiac myocytes and hyperplasia of cardiac fibroblasts. *Circ Res*. 1993;73(3):413–423.
24. Hsu YT, Youle RJ. Nonionic detergents induce dimerization among members of the Bcl-2 family. *J Biol Chem*. 1997;272(21):13829–13834.
25. Ago T, Kuroda J, Pain J, Fu C, Li H, Sadoshima J. Upregulation of Nox4 by hypertrophic stimuli promotes apoptosis and mitochondrial dysfunction in cardiac myocytes. *Circ Res*. 2010;106(7):1253–1264.
26. Ikeda Y, et al. Endogenous Drp1 mediates mitochondrial autophagy and protects the heart against energy stress. *Circ Res*. 2015;116(2):264–278.
27. Ago T, et al. A redox-dependent pathway for regulating class II HDACs and cardiac hypertrophy. *Cell*. 2008;133(6):978–993.